Layer Oriented Adaptive Optics: from drawings to metal

Farinato J.[a], Ragazzoni R.[ab], Diolaiti E.[c], Vernet-Viard E.[a],
Baruffolo A.[c], Arcidiacono C.[d], Ghedina A.[e], Cecconi M.[e],
Rossettini F.[f], Tomelleri R.[f], Crimi G.[g], Ghigo M.[g]

[a]INAF - Astrophysical Observatory of Arcetri, Largo E. Fermi 5,
I–50125 Firenze, Italy
[b]Max-Planck-Institut für Astronomie,
Königstuhl 17, D–69117 Heidelberg (Germany)
as W. Paul awardee by the Alexander Von Humboldt Societ
[c]INAF – Astronomical Observatory of Padova, Vicolo dell'Osservatorio 5,
I–35122 Padova, Italy
[d]Universita' di Firenze – Dipartimento di Astronomia e Scienza dello Spazio
L.go E. Fermi, 5 50125 Firenze, Italy
[e]Centro Galileo Galilei, Calle Alvarez de Abreu 70,
38700 Santa Cruz de La Palma, TF - Spain
[f]Studio Tecnico Tomelleri s.a.s., Viale del Lavoro 12/A
I–37069 Villafranca (VR), Italy
[g]Osservatorio Astronomico di Merate, via Bianchi 46,
I–23807 Merate (LC), Italy

ABSTRACT

In order to get first-hand results in the laboratory and possibly on the sky with the Layer-Oriented approach we designed, built, and tested a bread-board for this type of wavefront sensor. This device consists of a single wavefront sensor able to look simultaneously at four references. The positioning of three of the four reference stars with respect to the central one is made by the means of manually adjustable positioning units. A few additional degrees of freedom have been intentionally placed in the system in a way to test the sensitivity of the unit to misplacement and/or misalignment of some optical components. The laboratory set-up includes a crude system to mimic a telecentric F/32 focal plane illuminated by a number of fiber sources that can be placed in several different configurations. Wavefront deformation can be accomplished by placing some fixed deformating plates optically conjugated to several altitudes on the atmosphere. The system is designed in a way to be easily fitted to the existing AdOpt@TNG system, allowing for multiple references, one DM, closed loop operations. Preliminary results from this activity will be reported. Laboratory experiments includes checking of the theoretical predictions, especially the effectiveness in sensing up to a certain spatial frequency the layers not specifically conjugated to the detector. Results of a demonstrative experiment, showing how the wavefront sensor is able to disentangle layers contribution, are also reported.

Keywords: Layer Oriented, MCAO, Pyramid Wavefront Sensor, First MCAO WFS Prototype

1. INTRODUCTION

The extension of Adaptive Optics (AO hereafter) to Field of View (FoV hereafter) significantly larger than the isoplanatic patch size is a task accomplished by Multi Conjugated Adaptive Optics (MCAO hereafter) first envisaged by Beckers[1] and recently exploited in a number of different projects for 8m class telescopes (Gemini[2], LBT[3] and VLT[4] just to mention some of them).

Send correspondence to: Jacopo Farinato, E-mail: farinato@arcetri.astro.it

Adaptive Optical System Technologies II, Peter L. Wizinowich, Domenico Bonaccini,
Editors, Proceedings of SPIE Vol. 4839 (2003) © 2003 SPIE · 0277-786X/03/$15.00

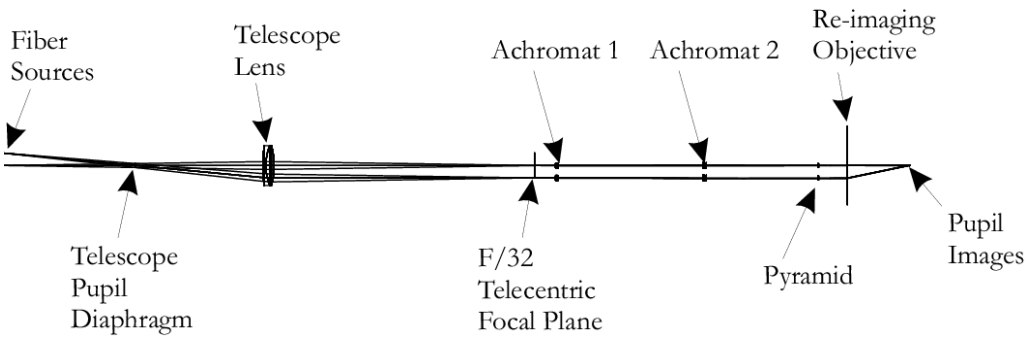

Figure 1. Optical layout of the breadboard prototype.

MCAO techniques, although realizing their purpose by the means of more than a single Deformable Mirror (DM hereafter) optically conjugated to different altitudes where different portions of the atmosphere can hence be compensated with great detail, differ substantially by the way the information to drive such DMs is retrieved and processed. MCAO requires, in fact, a wavefront sensing no longer confined to a single direction in the sky but to a realm of different sources, whichever artificial or natural.
In the first proposed MCAO concepts, and also in some on–going projects, several wavefront sensors, conventional in their concept, although especially designed for such a task, are coupled to one out of several point (or quasi- point, in case for istance of Laser Guide Stars) sources. In 1999[5], a different approach has been introduced, later defined in its detailed form[6,7] including variations on the theme like the Multiple Field of View[8,9] leading to expectations of even much better performances than what originally claimed.
In what has been called *layer–oriented* wavefront sensing, several stars are sensed simultaneously and optically coupled to a single detector conjugated to a specific altitude, or, in other words, to a specific layer. While we redirect the interested reader to other references for informations about finer details of this approach (some of these being likely still unveiled) we soon realized that the realization of a prototype in the laboratory for such a wavefront sensor could translate into a practical demonstration of the concepts embedded in the layer–oriented idea and also into the acquisition of a much deeper knowledge of the technicalities linked with this novel concept of wavefront sensor in order to have a much more detailed background for the design of on–sky experiments and instrument facilities, like NIRVANA[3] aboard LBT and one of the channels of MAD[4] aboard VLT.
In this framework we designed, built and tested a prototype of layer–oriented wavefront sensor that, although limited in the number of sensed stars and adopting manual stages for alignment and acquisition purposes, is conceptually identical to the ones we plan to implement on 8m class telescopes in the near future.

2. BREADBOARD OPTICS

The optical layout of the breadboard will be described in the following sections. We tried to use as much as we could off–the–shelf optical elements due to the very short time scale of the project.

2.1. Optical Layout

From the optical point of view, the prototype may be divided into two main sub-systems: a telescope model with a generator of *static turbulence* and a wavefront sensing module. The turbulence is measured by analyzing the light of four reference sources, represented by optical fibers with a 0.3mm core fed by a white light source. The optical layout is shown in Fig. 1.

Telescope–Atmosphere Model

The first sub-system includes the fiber sources, a diaphragm representing the telescope aperture (hereafter referred to as *telescope pupil diaphragm*), a set of screens to generate the static turbulence at various distances from the telescope pupil diaphragm and two lenses of focal length $f_0 = 160$mm (LINOS 322310), hereafter referred to as *telescope lenses*. The reference sources can be arranged in various configurations over a Field

of View FoV= 16mm in diameter, in order to simulate both regular and irregular star asterisms. The fibers are placed a distance f_0 to the left of the first telescope lens. The telescope pupil diaphragm is located a distance f_0 on the right of the first telescope lens and a distance f_0 on the left of the second telescope lens. With this arrangement the beams illuminating the turbulence screens are collimated, thus simulating a real situation where the reference sources are at infinite distance. Furthermore, the exit pupil appears at infinity. This sub-system delivers to the wavefront sensing unit a $F/32$ telecentric focal plane, where the images of the light sources are blurred by the turbulent screens.

WFSensing Unit

The wavefront sensing module consists of four star enlargers, each one ending with a pyramid prism, a re-imaging objective and a CCD detector to record the intensity on the re–imaged pupils. The star enlargers can be moved along two axes orthogonal to the system optical axis, in order to pick up the light of the simulated stars. From the optical point of view, the effect of the star enlargers is to magnify the images of the reference sources, increasing the focal ratio of each beam separately; the net effect is the shrinking of the pupil size on the detector plane. Each star enlarger ends with a pyramid prism which splits the light in four beams; the beams corresponding to the different sources are then optically combined by an objective, which produces in total four pupil images (one for each face of the pyramid prism) onto the detector. The perfect overlapping of the pupil images corresponding to the four reference sources actually occurs when the detector is conjugated to the telescope pupil diaphragm; when it is conjugated to a different screen, in fact, each pupil image splits in four slightly displaced pupils (one for each reference source), which can be accommodated into a circle called meta–pupil. Each star enlarger is formed by two achromatic doublets of focal length $f_1 = 25$mm and $f_2 = 150$mm respectively, increasing the focal ratio from the input value of $F/32$ to the final value of $F/192$. The first doublet is a commercial one (EDMUND 32305), while the second has been manufactured by Laboratorio Ottico Colombo. The pyramid prisms have been manufactured at the Osservatorio Astronomico di Brera-Merate by G. Crimi, grinding four BK7 commercial lenses; the nominal vertex angle ($\alpha = 1.2°$) ensures a suitable separation of the four meta–pupils when the detector is conjugated to the screens simulating the high–altitude turbulence. The re-imaging objective is a variable–focus commercial one (EDMUND 52585), with focal length $f = 75$mm and focal ratio $F/1.4$; adjusting the focus allows to conjugate the detector to different ranges, without moving its supporting system. The size s of each pupil image is given by $s = f/F$, where f is the focal length of the objective and F the focal ratio of the beams after the star enlargers ($F/192$); in our case, the individual pupil size results to be $s \approx 0.392$mm.

3. MECHANICAL DESIGN

The mechanical design of the prototype has been performed in the Osservatorio Astronomico di Padova and in Verona by Tomelleri SPA. In Fig. 2 the final system assembled in the lab is shown.

Due to the short time scale of the prototype, we tried to make the mechanical design as easy as possible in order to have the shortest possible delivery time for all the parts. We give now a brief description from the mechanical point of view of the sub-system of the prototype.

The first element is a mount holding an XY manual positioner which has the purpose to center the plate holding the optical fibers with respect to the central star enlarger of the 'star enlarger positioner '(that can be seen in Fig. 3). The fibers end with a standard SMA connector and they are fixed to the moving plate by using glue.
The second element is a commercial holder for a lens with the purpose to create a parallel beam in order to minimize distorsion effects on the turbulent screens. Immediately after there is the telescope pupil diaphragm, which is a custom made holder composed by two aluminium plates with a diaphragm simulating the telescope entrance pupil. Connected to it there are also two small aluminium plates holding the screens (that can of course be removed) used to introduce the turbulence at a certain altitude varying from 0km to about 20km.

Immediately after the pupil diaphragm there is the Telescope Lens Holder, supporting a lens of the same focal length of the first one (160mm), which is placed just before the Star Enlargers Positioner, the most complicated part of the mechanical sub-systems.

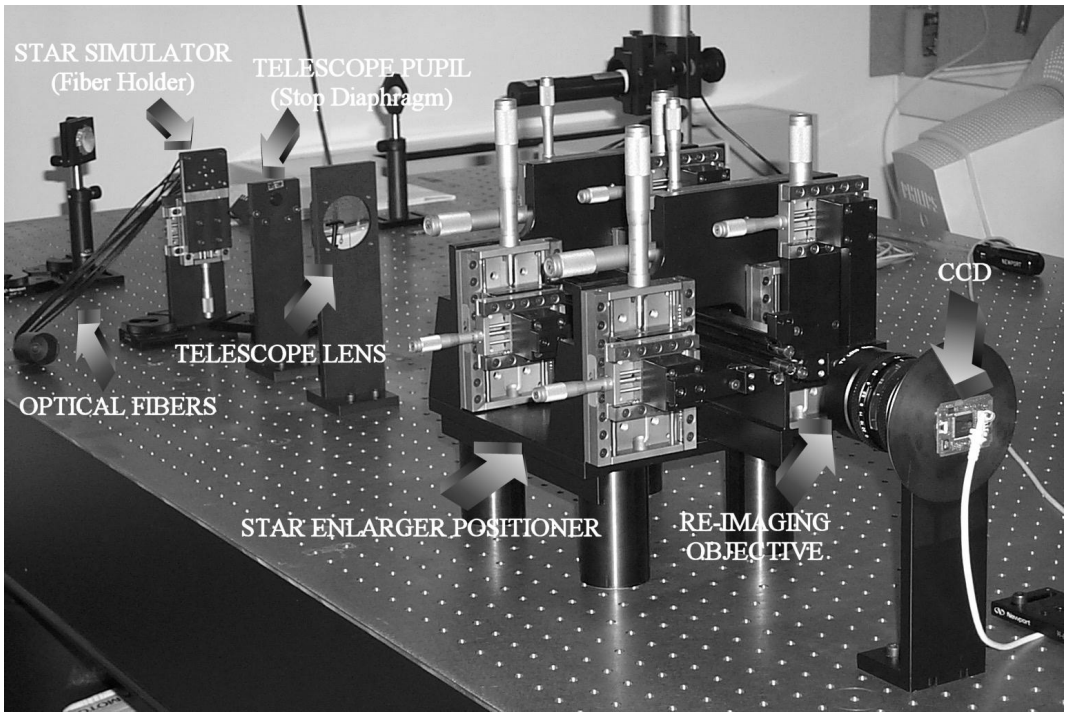

Figure 2. The complete system assembled in the lab.

The latter (shown in Fig. 3) is composed by a main base plate which is holding the rest of the mechanical structure. The base plate is kept at the proper beam height by four cylindric supports. Two plates mounted perpendicularly to the base plate have the purpose to hold the linear stages used to position the star enlargers. Every star enlarger is moved by two couple of XY linear stages, one for each end, in order to position them accurately with respect to the tip-tilt and to have a good superimposition of the 16 images of the pupil (4 each star enlarger because of the pyramids) on the detector. Every star enlarger end is connected to the XY movement through a thin elastic metallic plate which allows to move the two ends independently and moreover to adjust the focus of the star enlargers by using a screw connected to the movable part of the structure and pushing on the thin plate.

The four star enlargers are basically composed by an aluminium support as long as the distance between the first lens and the pyramid, with a shape done to accomodate the small cylindrical lens and pyramids mounts (glued on them); they are realised in a way to minimise their obstruction in the field, thus giving the possibility to have two star enlargers as close as the external diameters of the mounts of the bigger lenses, which is 8mm. The pyramid mounts allow the possibility to rotate the pyramid themselves, in order to give the possibility to tune their orientation.
The second last element of the system is the Pupil Re–Imaging Objective Holder (shown in Fig. 2), which is just before the CCD (we used an Electrim EDC-1000N) mounted on a commercial Tip-Tilt stage.

4. TURBULENT SCREENS CHARACTERIZATION

The atmosphere is simulated using several screens placed at different altitudes. We tested the quality in terms of phase degradation of different materials before to choose plastic layers. Seven 1.05 millimeter thick and 30×30 millimeter large screens have been characterized during a laboratory experiment measuring the Root Mean Square (RMS) of the different screens for several pupil masks by using an interferometer. From the RMS we computed an equivalent Strehl ratio which allowed us to estimate the perturbation of the screen. The second

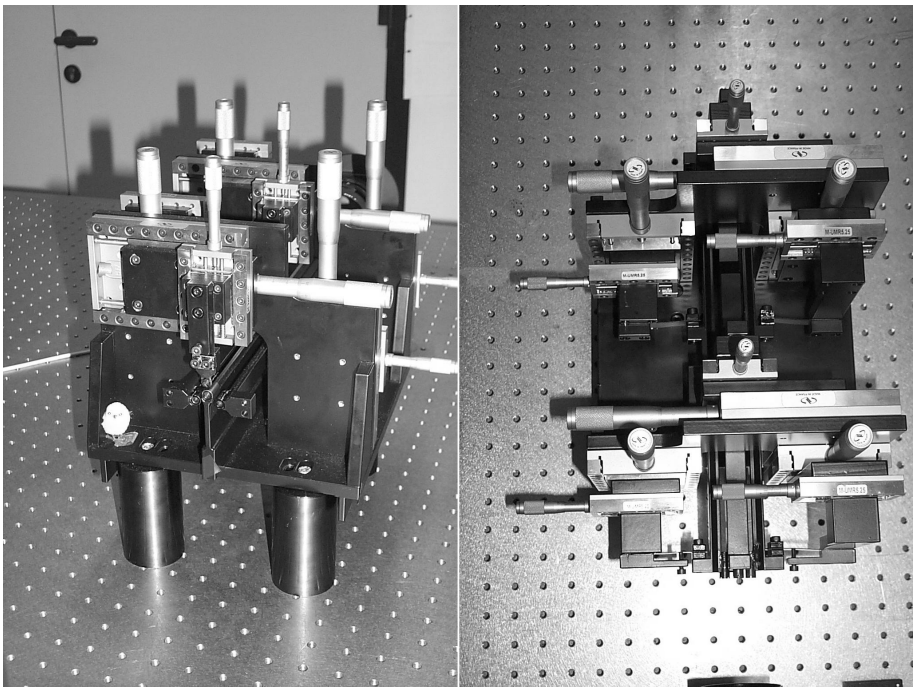

Figure 3. Two different views of the star enlargers positioner.

step in the characterization was the mapping of the wavefront itself and the decomposition of the wavefront on the Zernike basis. We obtained the wavefront of all the screens with several pupil diameters (the breadboard system has on the screens a pupil diameter of 3.2 mm on the ground and a metapupil diameter of 3.8 mm on the high layer). This characterization phase have been useful to validate the idea of using very simple screens as turbulent layers.

5. DATA REDUCTION SOFTWARE

Some procedures for the data analysis have been written in the IDL environment. The more relevant are listed below:

- `mask-abcd`: this procedure defines from the raw pupil images a bitmap, flagging the positions where the pupils lie. This defines four equal areas, which correspond to the footprint of the beams on the detector. While this is of a mere circular shape in the case of ground layer focusing, the shape is of course much more irregular in all the other cases.
- `signal`: this procedure simply performs the computation of the signal which is proportional to the wavefront derivative. It checks for division by zero and it can generate SNR maps in order to evaluate the quality of the signal over the footprint.
- `signal-to-wavefront`: the signal computed with the previous procedure is than used to compute the final estimated wavefront.
- `fitzernike`: this code can fit to the metapupil a number of Zernike polynomials, remove a certain amount, retaining a certain amount and so on. This is useful for both data reduction and diagnostic purposes.
- `BB_compu`: this procedure calls `signal`, `signal-to-wavefront` and `fitzernike`; it returns the wavefront image and its standard deviation either with or without the tip-tilt and defocus contributions.

6. TEST RESULTS: VALIDATION OF THE LAYER-ORIENTED CONCEPT

The first step with the system focused at a certain range was to take a measurement without any turbulent screen (Figure 4, left side). The goal was to retrieve the pupil masks used in all the further computations and to measure the so-called *static aberrations* of the system.

Figure 4. An example of static measurements obtained on the CCD when the system is focused either on the ground (1^{st} from the left) or around 6km (2^{nd} from the left). These measurements are used to determine the pupil masks (3^{rd} and 4^{th} from the left) but also to substract the static aberrations from the turbulent wavefront.

Figure 5. From the four pupil masks shown in Figure 4 right side, we compute the combined footprints. The imperfections of the pyramids degrade the recombination of the pupil masks: a part of the wavefront information is lost. The left side image shows the mask when the system is focused on the ground. The central image shows the 6km recombined mask. The right side image is the product of the two previous masks.

Figure 4 (right side, last two images) shows the masks obtained either for the ground or for 6km. The imperfections of the masks (cf Figure 5) is due to the bad quality of 2 out of 4 pyramids which introduce a considerable displacement of their corresponding four pupils. In the ideal case the four pupil footprints should be identical. The superimposition of the four groups of pupils is thus not perfect giving footprints differents for the four pupil masks. The right side mask of Figure 5 is used in paragraphs 6.2 and 6.3 to have a fair comparison between two wavefronts obtained with the system focused at different ranges. In all the following tests, the retrieved wavefronts have been processed subtracting the tip-tilt and defocus terms and all the units are homogeneous but arbitrary ones.

6.1. Focus on the ground (telescope pupil)

The first test was done using only one turbulent layer successively placed at different altitudes (equivalent scaled range of 0, 3, 6 and 9km) while the system was always focused at the ground level. The measurement allows to show the smoothing effect proportional to the distance between the layer of focusing and the turbulence layer altitude. The results are given in Figure 6. The RMS decreases significantly with the distance increase: moving the screen from 0 to 9km induces a drop of almost 50 percent of the RMS value.

In the second test we placed two turbulent screens respectively in position 1 (ground) and 2 (3km altitude) measuring the total wavefront. Then we measured the first screen alone, placed in position 1, and the second screen alone, placed in position 2 and seen out-of-focus, and we summed numerically the latter two separate measurements comparing the obtained result with the total wavefront measured with the two screens in position at the same time. The result of this test is shown in Figure 7: the RMS errors of the residual wavefront is lower than 1/10 of the wavefront amplitude.

The smoothing of a layer introduces a loss of its high frequency pattern. Hence, the farther the layer from the focusing altitude, the lower should be its contribution to the measured wavefront (only low frequency terms should remain). Leaving the system focused on the ground level, we measured the turbulence of the wavefront

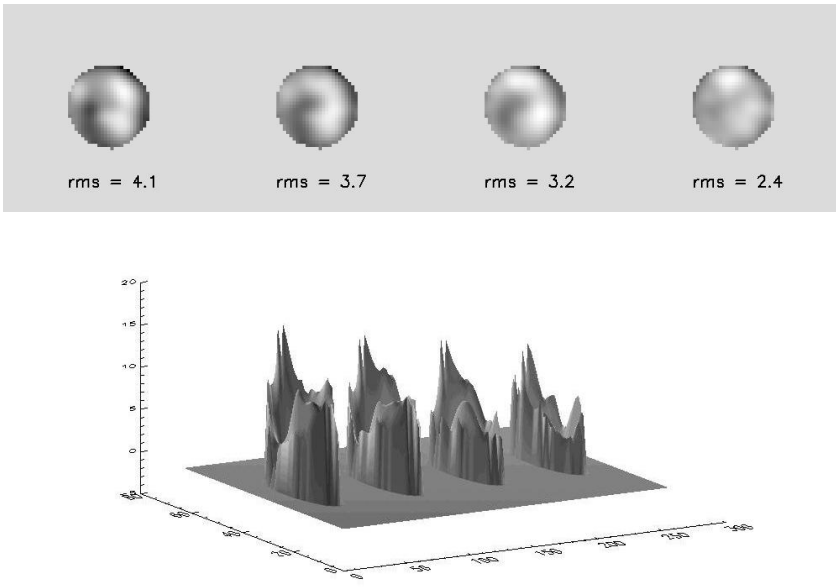

Figure 6. From the left to the right, the screen 4 is moved from the ground layer to an altitude of 9km using steps of 3km. In the upper image the wavefront maps are shown while the surface of the wavefronts is on the lower part. The RMS decreases gradually with the altitude increase. The wavefront smoothing is clearly shown in the surface view.

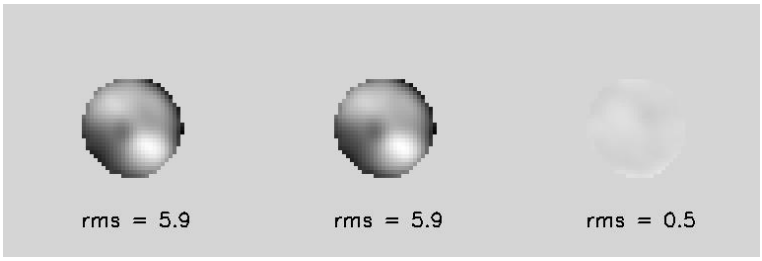

Figure 7. On the left side the wavefront is obtained by placing the screen 4 on layer 1, the screen 6 on layer 2 and by measuring the turbulence pattern. The central image is the sum of two wavefronts measured separetely (one wavefront with only the screen 4 on range 1, the other with only the screen 6 on range 2). The right-most image is the residual of the two.

for two screens. We placed one screen on the ground (at the WFS conjugation altitude) and we moved the other screen from altitude 2 to altitude 4. Figure 8 shows the result.

A layer-oriented system using a DM on the ground measures the ground turbulence layer and the low frequency terms on the high layer. The higher is the second layer, the lower are the frequencies sensed by the DM. A further verification of the smoothing effect was to compare the measurements obtained with two screens when inverting their positions. We used the screens 2 and 7 and measured the turbulence wavefront either with screen 2 on the ground layer and screen 7 on layers 2, 3, 4 or with screen 7 on the ground layer and screen 2 on the others layers. Figure 9 shows the wavefronts obtained. The higher left side and the lower left side wavefronts are almost identical as the higher right side and the lower right side wavefronts. This is again due to the smoothing effect of the turbulence layer far away from the altitude where the system is focused.

The following step is to verify the sensing when the system is focused at a high altitude layer and to see the effect of introducing a layer between the two altitudes of focusing.

The measurement of the non-conjugated layers is affected by a smoothing effect, with an associated cutoff

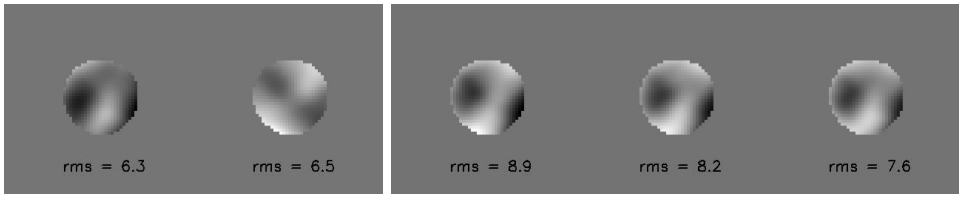

Figure 8. The left image shows the wavefront of the two screens used for this measurement when they are located on the ground. On the left side is shown the screen 3, on the right side the screen 6. Then the right side screen of the upper image is moved successively to different altitudes while the left side one stays on ground. The right image shows the corresponding three measurements. The total wavefront is always similar to the screen 3, which is seen in-focus, while the RMS decreases slightly, due to the smoother and smoother contribution of the other layer.

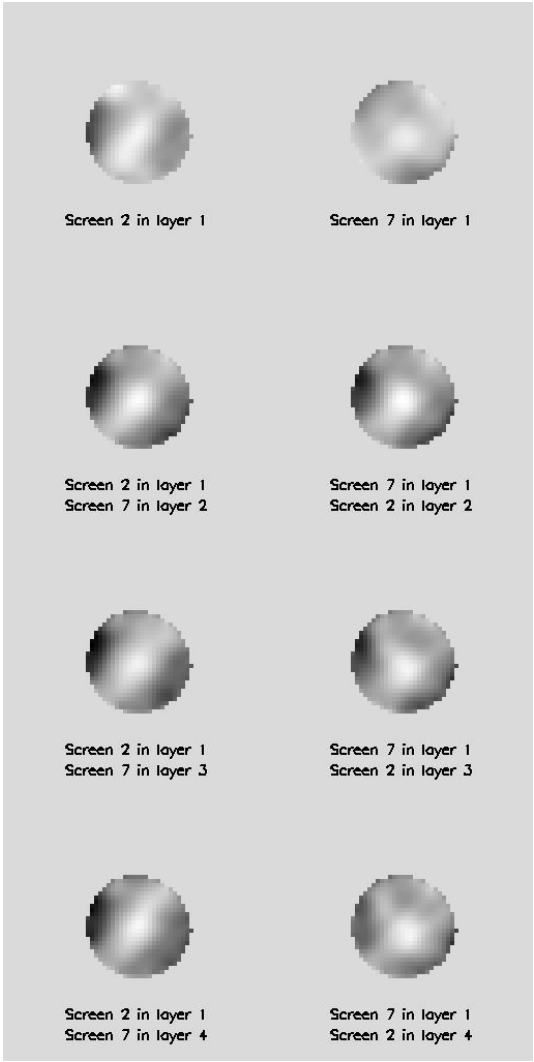

Figure 9. From the top to the bottom, we have on the left side, all the wavefronts obtained with the screen 2 on the ground and the screen 7 placed in layer 2, 3, 4; on the right side, the screen 7 always on the ground and the screen 2 placed on layer 2, 3, 4.

frequency inversely proportional to the difference in conjugation range and to FoV width. The best measurement would be the average of the non-conjugated layer wavefront over a region given by the FoV projected onto the layer itself. In any real MCAO system, the finite number of reference sources introduces a discretization of the FoV and therefore the wavefront averaging is not optimal. We performed a test to verify the accuracy of the wavefront measurement with only four reference sources, as compared to a FoV uniformly filled with guide stars. The ideal measurement in our test was numerically computed in the following way. Two screens were measured separately, placed on the ground layer with the system focused at the same position. Then the second layer was smoothed by a convolution with a uniform dish, whose width was equal to the projected FoV onto different non-conjugated layers. The first wavefront and the second after smoothing were then summed and compared to the measurement taken with *both* the screens in place, in particular with the first screen in focus at the ground layer and the second moved from layer 2 to layer 4. The results of the tests are shown in Figure 10: the measured wavefront is very similar to the ideal measurement.

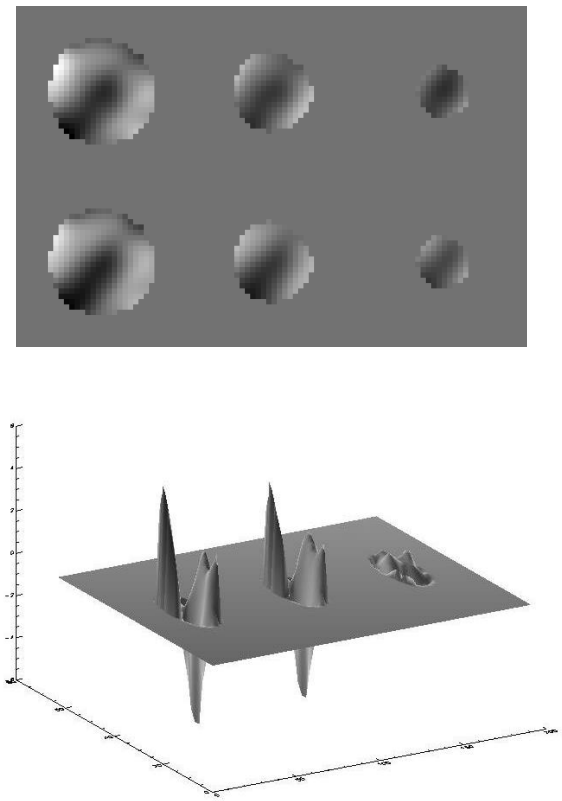

Figure 10. The above image shows three measured wavefronts with one screen always in layer 1 and another screen in layers 2, 3 or 4 (top row); these are compared to the ideal measurement, given by the first layer plus a smoothed version of the second, computed by convolving the screen with a uniform dish of increasing width (bottom row). The useful region of the ideal measurement becomes smaller as the distance of the non-conjugated layer increases: this is related to the numerical convolution. The bottom image shows a different view of the first case (one screen in layer 1 and the second in layer 2); the residual between the measured and the computed wavefront is shown on the right side.

6.2. Focus either on the ground or around 6 km

The screen 6 was located on the ground while the screen 3 was in layer 3, around 6 km. The system was first focused on the ground and the wavefront obtained is similar to the screen 6. Then by changing the altitude of focusing to layer 3 at 6 km we can see that the wavefront obtained is similar to the screen 3. We inserted also two different screens (screen 2 which has a low RMS value and screen 1 which is stronger in terms of RMS) on

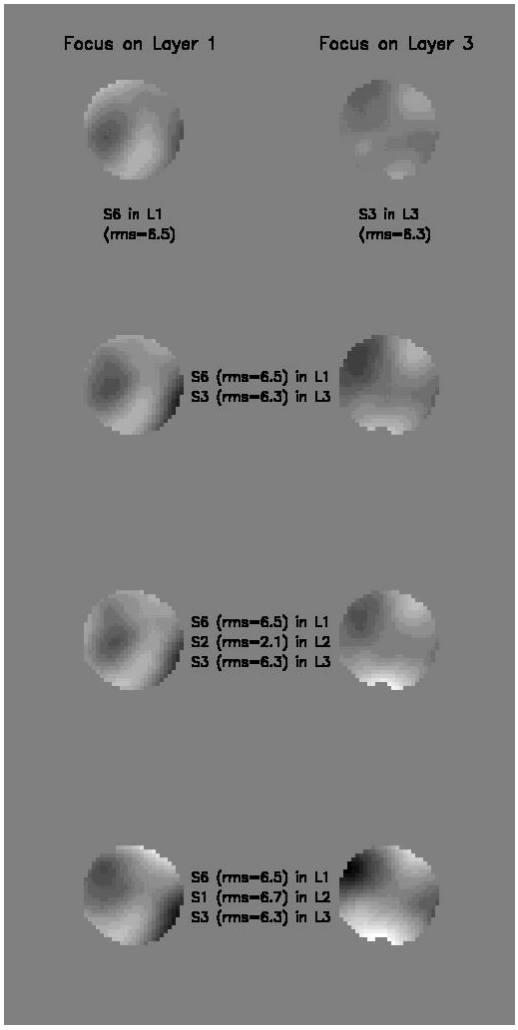

Figure 11. The screen 6 is located on the ground while the screen 3 is in layer 3, around 6 km. The third and fourth rows show the effect of introducing a third turbulent layer between the other two.

the layer 2 (3 km in altitude) between the two altitudes of focusing and checked their effects on the measured wavefront.

Figure 11 summarizes the various properties of the layer-oriented measurement in open loop when using two altitudes of sensing. If the atmosphere is composed of two layers located at the altitudes of sensing, the ground CCD measures mainly the ground turbulence while the high layer CCD measures mostly the high turbulence layer. But the two CCDs measure also the low frequency terms of the other layer. A layer situated at an intermediate altitude will be seen smoothed by the two CDDs.

6.3. Focus at 0, 3 or 6km

We finally checked the measured wavefront obtained focusing the system on layers 1, 2 and 3, with three screens in place at these positions. The result is shown in Figure 12. The aim of this test is to show that the sensor is always more sensible to the turbulent layer placed at the WFS conjugation altitude.

In order to ensure the matching of the total measured wavefronts with the screen in the conjugated layer, we computed the correlation coefficients of the measurements (Table 1). Such correlation figures are always

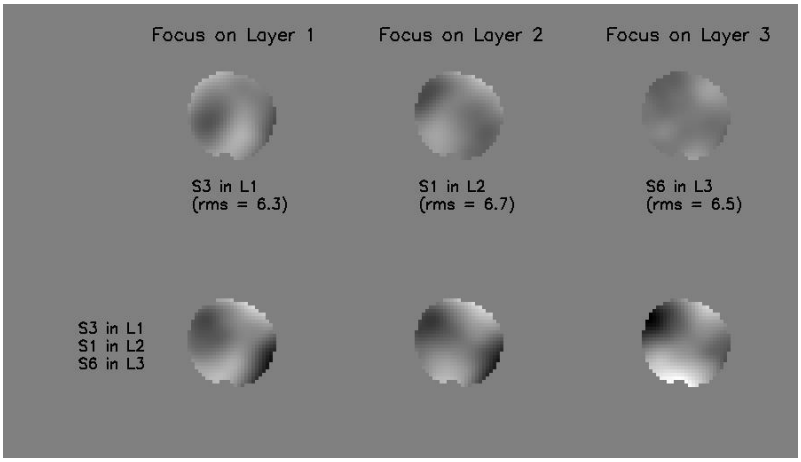

Figure 12. The upper three images show the wavefront of the screens 3, 1 and 6 measured alone with the system focused to the layers 1, 2 and 3 respectively. The lower three wavefronts are obtained with all the three screens in place, for different conjugation ranges of the system.

Correlation	Screen 3 in focus on layer 1	Screen 1 in focus on layer 2	Screen 6 in focus on layer 3
Screen (3 + 1 + 6) focus on layer 1	0.44	0.74	0.55
Screen (3 + 1 + 6) focus on layer 2	0.27	0.83	0.65
Screen (3 + 1 + 6) focus on layer 3	0.13	0.70	0.70

Table 1. Correlation coefficients computed between the different wavefronts presented in Figure 12. Each wavefront obtained with three turbulence screens in place while focusing on three different altitudes is correlated with the three single screens focused at one of the three layers.

much larger than zero. In order to get a proper loop closure it is enough to have any positive correlation between the total observed wavefront and the true one. The larger is the correlation the faster will be the bootstrapping phase. In fact, as soon as the correlation is larger than zero the corresponding layer will be removed, improving the correlation of the other layer–oriented loop. The viceversa holds as well. The condition for bootstrapping the loop is therefore a non-negative correlation. In all the observed cases we experienced a safely positive correlation. For each column in the Table the correlation between the total wavefront and a given screen properly reaches a maximum at the specific range where the screen is located. For istance it is larger at 6km rather than 3km or at the ground level if the considered screen is at 6km. The correlation between the Screen 3 and the total wavefront when the system is focused on layer 1 is the worse (0.44). Two different effects can explain this result: first the screen 3 has a RMS value lower than the other screens. In addition, the low frequency wavefront patterns of the screens 1 and 6 are similar: the low order terms added to the Screen 3 are 'amplified'. But even under such conditions, the correlation coefficient is by far higher than zero.

7. CONCLUSIONS

For the first time we built in the laboratory a wavefront sensor measuring collectively the light coming from four different sources. There are no conceptual limit to the number of the observable stars, other than optomechanical issues. The light carrying information upon the turbulence or the wavefront perturbation from their origin to the entrance of the wavefront sensor has been successfully coadded optically and fed into a single detector. The data analysis performed shows that the system behaves qualitatively as predicted.

The Breadboard system validated the most important principles of the layer-oriented concept. Especially:

- The correct behaviour of the layer–oriented wavefront sensor has been demonstrated by observing several configurations with up to 3 layers at different focusing altitudes;
- The proper smoothing of the layers has been checked with an accuracy at least better than $\approx 10\%$;
- The proper re–imaging of a specific layer, as seen through two perturbing screens, has been accomplished with correlation coefficients in the range 0.4 ... 0.85.

A more quantitative characterization of the results must be done soon in order to express the numerical results with the proper units, even if already now there is evidence of the proper behaviour of the system (see Table 1).

We are testing in these days 4 new pyramids made with a completely different technology[10] that look more reliable in term of optical quality of the final elements and also in term of repeatibility. New tests are foreseen in the next days.

A number of *lessons learned* have been used to improve either the alignment issues or the mechanical design of future WFS LO based like ESO–MAD.

Acknowledgements

Many thanks to Giancarlo Farisato for the assembly of the two set of fibers that we used for the experiment, to Paolo Stefanini for the fantastic support in solving every mechanical problem we had to face and to Laboratorio Ottico Colombo for the manufacturing of the lenses of the star enlargers. Thanks are due also to Piero Salinari, Simone Esposito, Armando Riccardi, Alfio Puglisi, Marcel Carbillet, Christophe Verinaud, Sandro Gennari and Carlo Baffa for the support and the useful suggestions during the assembly, integration and test phase.

Bibliography

1. Beckers J.M., SPIE Proceedings 1114, 215, 1989
2. B. L. Ellerbroek, F. J. Rigaut, C. Boyer, C. DOrgeville, M. R. Hunten, "Multiconjugate adaptive optics for Gemini-South", Adaptive Optics System Technologies, SPIE Proceedings, 4839, article number [4839-07], 2002.
3. R. Ragazzoni, T. Herbst, D. Andersen, P. Bizenberg, H.W. Rix, R-R. Rohloff, C. Arcidiacono, E. Diolaiti, S. Esposito, J. Farinato, A. Riccardi, E. Vernet-Viard, P. Salinari, "NIRVANA: a visible MCAO channel for LBT", this Conference.
4. E. Marchetti, N.N. Hubin, E. Fedrigo, R. Donaldson, R. Conan, M. Le Louarn, B. Delabre, F. Franza, D. Baade, C. Cavadore, A. Balestra, J.-L. Lizon, R. Ragazzoni, J. Farinato, E. Vernet-Viard, E. Diolaiti, D.J. Butler, S. Hippler, A. Amorin, "MAD: the ESO multiconjugate adaptive optics demonstrator", this Conference.
5. Ragazzoni R., ESO Conference and Workshop Proceedings, 57, 175, 2000
6. Ragazzoni R., Farinato J., Marchetti E., SPIE Proceedings 4007, 1076, 2000
7. Diolaiti E., Ragazzoni R., Tordi M., A&A, 372, 710, 2001
8. Ragazzoni R., Diolaiti E., Farinato J., Fedrigo E., Marchetti E., Tordi M., Kirkman D., A&A accepted, 2002
9. Ragazzoni R., Diolaiti E., Farinato J., Fedrigo E., Marchetti E., Tordi M., Kirkman D., Venice Conference Proceedings, 2002
10. M. Ghigo, F. Perennes, R. Ragazzoni, "Manufacturing by deep x-ray lithography of pyramid wavefront sensors for astronomical adaptive optics", this Conference.